

A close binary nucleus in the most oxygen-poor planetary nebula PN G 135.9+55.9.

G.H. Tovmassian

*Observatorio Astronómico Nacional, Instituto de Astronomía , UNAM,
P.O. Box 439027, San Diego, CA 92143-9027, USA
gag@astrosen.unam.mx*

R. Napiwotzki

*Department of Physics & Astronomy,
University of Leicester, University Road, Leicester LE1 7RH, UK
rn38@astro.le.ac.uk*

M. G. Richer *

*Observatorio Astronómico Nacional, Instituto de Astronomía , UNAM,
P.O. Box 439027, San Diego, CA 92143-9027, USA
richer@astrosen.unam.mx*

G. Stasińska *

*LUTH, Observatoire de Meudon, 5 Place Jules Janssen, F-92195 Meudon Cedex, France
grazyna.stasinska@obspm.fr*

A.W. Fullerton**

*Department of Physics and Astronomy, University of Victoria,
P.O. Box 3055, Victoria, BC V8W 3P6, Canada
awf@pha.jhu.edu
and*

T. Rauch

*Institut für Astronomie und Astrophysik Tübingen (IAAT) Abteilung Astronomie
Sand 1 D-72076, Tübingen, Germany
rauch@astro.uni-tuebingen.de*

ABSTRACT

We report FUSE¹ and new deep optical spectroscopic observations of PN G 135.9+55.9, the most oxygen-poor planetary nebula located in the Galactic halo. These observations allow us to estimate the gravity of the central star by fitting the profile of the observed H I absorption lines with NLTE model atmospheres. Our best fit implies that the central star is still in a pre-white dwarf stage. We also find large variability of the radial velocities of the absorption component of the Balmer lines on a timescale of hours. This is direct evidence that the nucleus of PN G 135.9+55.9 is a close binary. The large semi-amplitude of the radial velocity variations and the probably short period suggest a massive compact companion, likely a white dwarf. Although our orbital solutions are very preliminary, they indicate that the total mass of the system probably exceeds the Chandrasekhar limit. If confirmed, this would make this binary the potential progenitor of a type Ia supernova.

Subject headings: ISM: planetary nebulae; individual: central star; Ultraviolet; ISM: spectroscopy;

1. Introduction

PN G 135.9+55.9 (also called SBS 1150+599A) is a recently discovered planetary nebula in the Galactic halo (Tovmassian et al. 2001) whose oxygen abundance is reported to be extremely low, of order 1/100 of the solar value or less (Tovmassian et al. 2001; Richer et al. 2002; Jacoby et al. 2002). This makes it, by one order of magnitude, the most oxygen-poor planetary nebula known so far. Such a low oxygen abundance may be either genuine and represent the oxygen abundance in the material from which the progenitor star formed, or it may be the result of mixing processes while the star was on the AGB. Although the presently available determinations of the Ne/O ratio are discrepant by a factor of about 10 (Richer et al. 2002 and Jacoby et al. 2002), they indicate that, even in the case of conversion of O into Ne, the original oxygen abundance of the progenitor of PN G 135.9+55.9 is likely extremely low.

Clearly, this unique object deserves a more detailed study to better define its nature. Tovmassian et al. (2001) speculated upon various scenarios for the formation of this planetary nebula. One of them assumed a progenitor star having formed out of infalling material. Another invoked the existence of a close binary core. In this paper we focus on the information provided by new observations concerning the nature of the central star of PN G 135.9+55.9. A companion paper (Stasińska et al. in preparation) will discuss new observational constraints on the chemical composition of this object.

First, we acquired far-ultraviolet spectra of PN G 135.9+55.9 using the Far Ultraviolet Spectroscopic Explorer (FUSE). We also obtained a series of high signal-to-noise optical spectra of the nebula and its central star. From these observations, one can constrain the fundamental parameters of the central star. It is also possible to investigate whether there might be variability on short time scales. The most surprising result of our study is the discovery that the core of this planetary nebula is a short period, close binary with an unseen companion, probably a white

dwarf.

The paper is organized as follows: In Section 2, we describe the observations and the reduction procedure, both for the FUSE and ground-based observations. In Section 3, we describe the main spectral features of the object from the FUSE and ground-based observations. In Section 4, we present a stellar atmosphere analysis that allows us to infer the gravity of the ionizing star from the observed H I absorption features and estimate parameters of the binary system. In Section 5, we present estimates of the reddening of PN G 135.9+55.9 based upon the FUSE data and in Section 6 we estimate the distance and age of PN G 135.9+55.9. In Section 7, we discuss the binary nature of the core and the masses of its components. Finally, in Section 8, we summarize the main results of this study and present some prospects for future study.

2. Observations

2.1. FUSE observations

FUSE is an orbiting observatory with the capability to obtain high resolution spectroscopy in the wavelength region between 900 and 1200 Å. It consists of four co-aligned telescopes optimized for far-UV wavelengths. The spherical, aberration-corrected, holographic diffraction gratings disperse light from four channels. Two channels with SiC coatings cover the 905–1100 Å region and two others with Al+LiF coatings detect the 1000–1187 Å range. An overview of the FUSE mission has been given by Moos (2000).

The observation of PN G 135.9+55.9 (ID# C034) was conducted through the LWRS aperture (30'' × 30'' square) on 2002 January 30 for a total exposure time of 30 660 s. The observation was composed of seven individual integrations of approximately 4200 s each, simultaneous in all channels. These observations were among the first executed after the recovery from the failure of two reaction wheels in December 2001. Therefore, the pointing was not as good as was achieved before the accident or after the situation was taken under complete control. We have checked possible deviations during the observations. There was a systematic, quasi-sinusoidal pointing drift on an orbital time-scale. However, the maximum displacement is only 2''.3, which corresponds to

*Visiting Astronomer, CFHT

**Center for Astrophysical Sciences, Department of Physics and Astronomy, Johns Hopkins University, 3400 North Charles Street, Baltimore, MD 21286, USA

a maximum shift of 0.026 \AA (i.e., 7.7 km/s at 1000 \AA), or about half a spectral resolution element. Thus, it can hardly pose a problem, but the pointing itself (centering in the aperture), which is difficult to verify, can introduce zero-point offsets of up to 0.15 \AA . The pipeline reduction package CalFUSE 2.1.7 was used for the extraction of the spectra as well as reduction and calibration purposes.

Our examination of the spectra showed that the wavelength shifts between individual exposures, which are common for FUSE data, never exceeded 1.5 pixels and were usually in the 0.1–0.5 pixel range. Since the shifts were negligible, we used a non-standard processing wherein all 7 exposures were concatenated into one large photon list before pushing it through CalFUSE 2.1.7. This permits a more reliable background model to be created, which is especially important for faint targets such as PNG 135.9+55.9, and also eliminates the need to cross-correlate and coadd exposures. The other important procedure that we used was to separate the night exposure (NE) from the total exposure of the object. The data are severely contaminated by the airglow lines arising from the illuminated atmosphere of the Earth during day time (Feldman et al. 2001). In order to eliminate the strong emission lines from the terrestrial airglow, we extracted photons obtained when the exposure was taken during orbital night. This decreased our exposure time by factor of 3. We use both the total exposure and NE spectra to analyze the data of PNG 135.9+55.9. No event bursts or other unusually strong glitches common for FUSE data were detected in the raw images or the photon arrival rate plots (see The FUSE Instrument and Data Handbook edited by Sahnou et al. 2002).

2.2. CFHT optical observations

The observations at the Canada-France-Hawaii Telescope (CFHT) were obtained on 2003 May 1 UT with the MOS spectrograph (Le Fèvre et al. 1994). The U900 grism was used to observe the $3400\text{--}5300 \text{ \AA}$ spectral interval. A $1''$ slit was used. Coupled with the EEV1 CCD, $2048 \times 3900 \times 13.5 \mu\text{m}$ pixels, the dispersion was 0.78 \AA/pix and the resolution $3.0\text{--}3.5 \text{ \AA}$, based upon the widths of arc lamp lines. A B filter (CFHT filter #1412) was used to center the central star of PNG 135.9+55.9 in the slit. The spec-

tra of PNG 135.9+55.9 were obtained in pairs with the spectrograph slit set at the parallactic angle corresponding to the midpoint of the pair of spectra. This was done since the spectrograph rotation and object re-acquisition took a significant amount of time. For the observations of PNG 135.9+55.9 and the standard star BD+33°2642 (Oke 1990), the slit position angle was within 10° of the parallactic angle at all times. Seven 1800s exposures of PNG 135.9+55.9 were obtained spanning the airmass range 1.30–2.65. The observations of BD+33°2642 were obtained using a $5''$ slit. Spectra of Hg, Ne, and Ar lamps were obtained for wavelength calibration at the end of the night only. Images of the flat field lamp were obtained through both slits to correct for pixel-to-pixel variations. Bias images were also obtained in order to remove any two-dimensional structure in the bias level.

The data were reduced using the Image Reduction and Analysis Facility (IRAF)² software package (specifically the *specred* package). The mean level of the overscan region was subtracted from each image. Next, the average of the overscan-corrected bias images was subtracted from all object and flat field images to remove any two-dimensional bias structure. The flat field images were combined and then processed to divide out the shape of the flat field lamp. The resulting flat field was then divided into all object images. The spectra of PNG 135.9+55.9 and the standard star were extracted to one-dimensional images, subtracting the sky contribution by defining sky apertures on both sides of the object spectra and interpolating between them with a straight line. The wavelength axis was calibrated using the spectra of the arc lamp. Since the object was observed repeatedly over a large airmass interval, an empirical atmospheric extinction curve was derived from the data. This extinction curve turned out to be somewhat steeper than that given in the CFHT Observatory Manual³. The spectra were calibrated in flux using the observations of the standard star and the previous empirical atmospheric extinction curve. The individual spectra of PNG 135.9+55.9 were completely calibrated be-

²IRAF is distributed by the National Optical Astronomical Observatories, which is operated by the Associated Universities for Research in Astronomy, Inc., under contract to the National Science Foundation.

³See <http://www.cfht.hawaii.edu/Instruments/ObservatoryManual/>

fore combining or further analyzing them.

3. The main features of the observed spectra

The FUSE spectrum itself is an approximately flat continuum, with a mean level of about $3 \times 10^{-14} \text{ erg s}^{-1} \text{ cm}^{-2} \text{ \AA}^{-1}$. There are many lines of interstellar (IS) H_2 . No emission lines could be seen except those that are definitely associated with terrestrial airglow. Most of these lines disappear in the NE spectrum, with only the strongest lines of H I and O I leaving residual emission peaks whose intensities are dramatically reduced compared to the all photon spectrum. Since the systemic velocity of PN G 135.9+55.9 is -193 km/sec (Tovmassian et al. 2001; Richer et al. 2003), there is no possible confusion between airglow emission lines and lines from the object. The FUSE NE spectrum of PN G 135.9+55.9 is presented in Fig 1. On the whole, it is impressively featureless, particularly when compared with a large subset of FUV spectra of planetary nebulae from the FUSE archives that we examined. This remarkable absence of features in the FUSE spectrum of PN G 135.9+55.9 is consistent with the very low metal abundances derived from the analysis of the PN.

3.1. Absorption lines from the interstellar medium in the FUSE spectrum

Most of the absorption lines that are observed originate in the interstellar matter between us and the object. There are numerous lines of molecular and atomic hydrogen. Their study can provide interesting constraints upon the distribution of H and H_2 along the line of sight toward the object (see e.g. McCandliss 2003). However, we are mainly concerned with the physics of PN G 135.9+55.9 itself in this paper and discuss only the impact of these interstellar lines upon our analysis of PN G 135.9+55.9.

Molecular hydrogen is a significant source of contamination when studying the spectral features of the underlying source. Fortunately, the physics of absorption by molecular hydrogen is well understood and can be reliably modeled. Absorption bands of interstellar molecular hydrogen arise from the photo-excitation of molecular hydrogen by the background continuum object, causing elec-

trons in the ground electronic state to be excited into higher states of either the Lyman or Werner bands. The strength of these absorption lines is proportional to the molecular column density distribution within the ground electronic state's rotational (J'') and vibrational (v'')² energy levels along a particular line-of-sight. We used the FUSE Simulator Tool to model the FUSE spectrum (<http://violet.pha.jhu.edu/~gak/fwebsim.html>).

In order to estimate the hydrogen column density, we used a flat spectrum of intensity $3 \times 10^{-14} \text{ erg s}^{-1} \text{ cm}^{-2} \text{ \AA}^{-1}$ and a variety of parameters for the foreground column densities of atomic and molecular hydrogen. Later, we repeated this analysis with our derived model spectrum, described in the following sections, and obtained exactly the same results. A grid of values of neutral hydrogen column densities ranging from $\log N_{\text{H}} = 20$ to 20.6 cm^{-2} were investigated. For H_2 , the input values were $\log N(v'', J'') = 18$ to 20. The model uses Voigt profiles to calculate the optical depth variation with wavelength for each line. Line shapes reproducing the linear, flat, and square root portions of the curve-of-growth are controlled through the specification of the Doppler parameter b . The Doppler parameter b of line width was adopted equal to 10 km s^{-1} , as provided by default in the simulation tool.

The modelled interstellar absorption shows a significant 0.2 \AA wavelength shift compared to the observed spectrum as estimated from cross-correlation. This shift is larger than expected for interstellar hydrogen absorption, e.g., Bannister et al. (2003) did not measure velocities in excess of 30 km/s for interstellar lines from atomic species in a sample of white dwarfs with high resolution HST UV spectra. Even considering the much larger distance to PN G 135.9+55.9 compared to that sample, it is unlikely that the entire wavelength shift is due to high velocity clouds along this line of sight. At least half of the shift in the FUSE spectrum of PN G 135.9+55.9 (0.2 \AA corresponds to approximately 60 km/sec) is probably caused by imperfect centering of the central star in the LWRs aperture of FUSE. This is a well-known problem that can cause shifts of the wavelength scale. We adopted the view that the radial velocity shift of the H_2 features is caused by this instrumental effect and corrected the wavelength scale for further fitting of the photospheric line

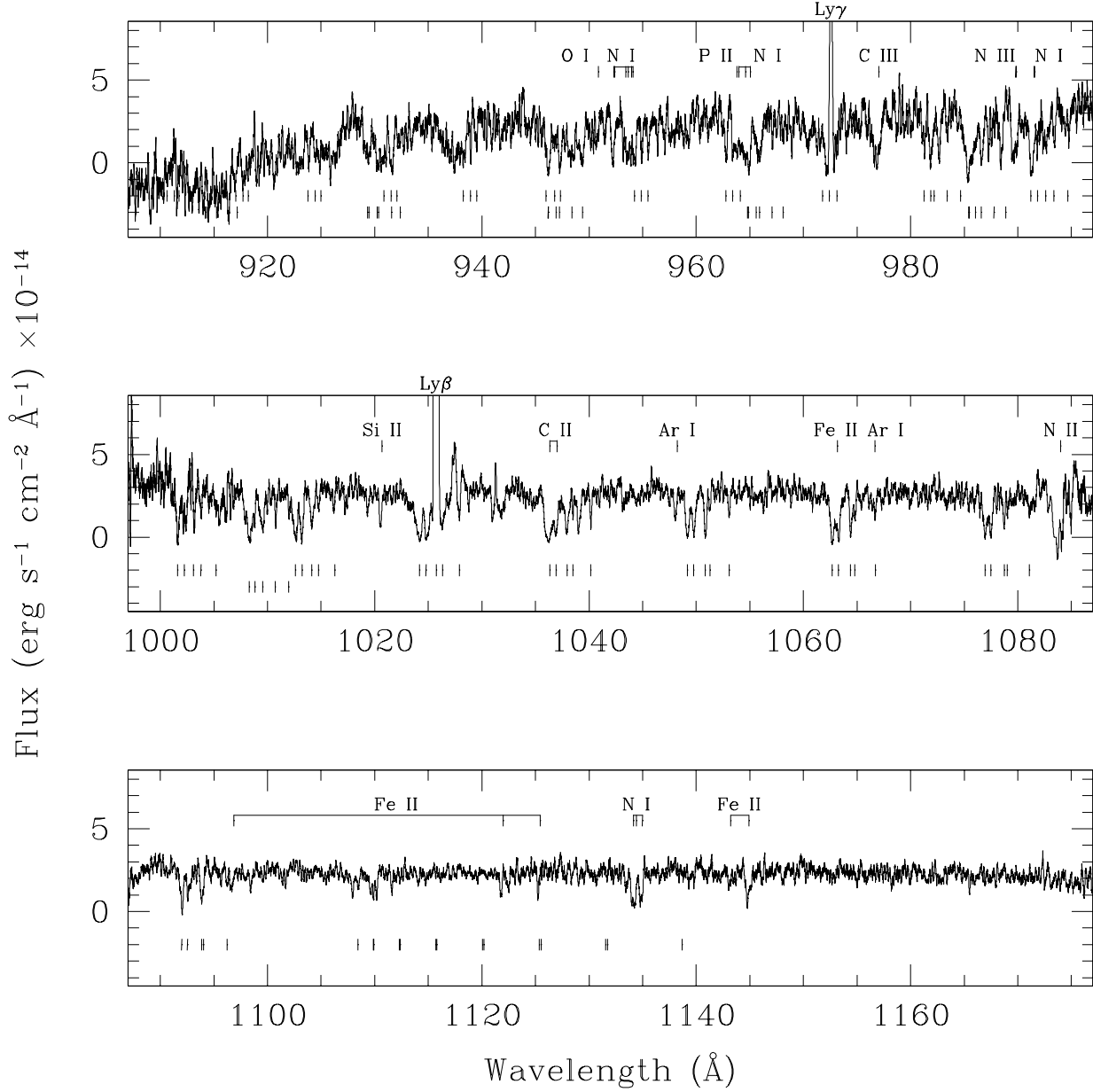


Fig. 1.— The FUSE composite spectrum of PNG 135.9+55.9 for the night only exposure. A few of the strongest H I and O I $\lambda 1025.76 \text{\AA}$ airglow lines remain in emission. The other features are absorption lines, most of which are due to interstellar matter. Molecular hydrogen lines are marked along the bottom of the spectrum: the tick marks for the Lyman series lines are above those for the Werner series. Some other prominent interstellar lines of other elements are marked above the spectrum. The rest positions of Ly β and Ly γ are marked above the corresponding boxes.

profile.

The H_2 column density strongly affects the profiles of the H_2 lines, whereas the impact of the neutral hydrogen column density is less significant. In Fig. 2 simulated spectra with different hydrogen ($H I$, H_2) column densities are presented. Two spectral regions are shown. The first is around $\lambda 1012 \text{ \AA}$, where the Werner series has strong lines, while the other is around $\lambda 1108 \text{ \AA}$, with prominent H_2 lines of the Lyman series. In both regions, even without doing a χ^2 fit, it is obvious that values of $\log N_{H_2}$ of 18 and 20 dex are far from fitting the observed line profiles and intensities, while $\log N_{H_2} = 19$ dex provides a good fit. For neutral hydrogen, the choice of the best fit is not so obvious. Another useful web tool allows one to calculate the column density depending upon the direction in the Galaxy based upon the results of Dickey & Lockman (1990, <http://heasarc.gsfc.nasa.gov/cgi-bin/Tools/w3nh/w3nh.pl>). According to this calculation, the expected neutral hydrogen column density is $N_H \approx 1.53 \times 10^{20} \text{ cm}^{-2}$ in the direction of PNG 135.9+55.9. This roughly corresponds to the modelled value of $\log N_H = 20.3$, which is shown in the second panel from the bottom in Fig. 2. However a higher value of $\log N_{H_2} = 20.6$ seems to be an equally good fit. We suspect that the column density toward PNG 135.9+55.9 may be slightly higher than 20.3 dex, as follows also from the analysis of absorbed flux in the UV. This will be discussed in detail below in Sect. 5.

Besides the numerous H_2 lines of the Werner and Lyman series, there is a large number of absorption lines from O I, N I, N II, N III and Fe II that are also due to the intervening interstellar medium. These lines are commonly encountered during FUSE observations (e.g. Froning et al. 2001; Wolff et al. 2001) and, most importantly, their wavelengths indicate that they are not related to our object. The fact that these lines are numerous and strong is in agreement with the previously deduced large distance to the object and its location in the Galactic Halo (Tovmassian et al. 2001; Richer et al. 2002, see also Sect. 6).

3.2. Hydrogen and helium features physically related to PNG 135.9+55.9

The only spectral feature in the FUSE spectrum firmly identified to arise in our object, apart

from the continuum, is the relatively broad absorption from $Ly\beta$ that we attribute to the central star. The only possible emission feature from the nebula itself is a small emission peak inside the $Ly\beta$ absorption. As mentioned above, we expect the lines from the central star to be Doppler shifted to the blue by the heliocentric systemic velocity of the nebula, -193.3 km s^{-1} (Richer et al. 2003). The nebular lines may appear to be blue-shifted somewhat more, to as much as -205 km s^{-1} , because the nebular emission consists of two components with the blue-shifted component being the stronger of the two (Richer et al. 2003). The portion of the all photon spectrum around $Ly\beta$ is presented in Fig. 5 along with the models that were fit to it (described below).

The profile of the absorption feature blueward of the vacuum wavelength position of $Ly\beta$, indicated by a strong airglow line, is extremely complicated. First, the absorption line is saturated. Second, the red wing is contaminated by the airglow emission whose profile itself is complicated by a small glitch on the blue wing. Third, there is residual emission from the O I airglow line further to the red. Fourth, there are several strong components of interstellar H_2 Lyman lines inside the stellar absorption line. Finally, inside the absorption feature sits an emission peak that we interpret as nebular He II 6-2 $\lambda 1025.273$ emission (see below) superposed upon the H I $Ly\beta$ absorption feature from the central star. The emission line that we identify as He II has a measured wavelength of 1024.57 \AA . This coincides exactly with the position of He II $\lambda 1025.273$ at a radial velocity of -205 km s^{-1} .

We corrected the line profile in the all photon spectrum, applying the model of interstellar absorption with the parameters estimated in the previous section ($\log N_H = 20.3$ and $N_{H_2} = 19$). The residual spectrum still shows broad photospheric $Ly\beta$ absorption as well as emission at the position of He II line. Although the strength of the absorption feature corresponding to $Ly\beta$ depends upon the parameters adopted for interstellar hydrogen in the model, it is both expected and present in the spectrum. We are less confident regarding the He II emission feature, because it is located in a gap between two strong interstellar lines and can be easily confused with the residual intervening continuum. However this supposed emission

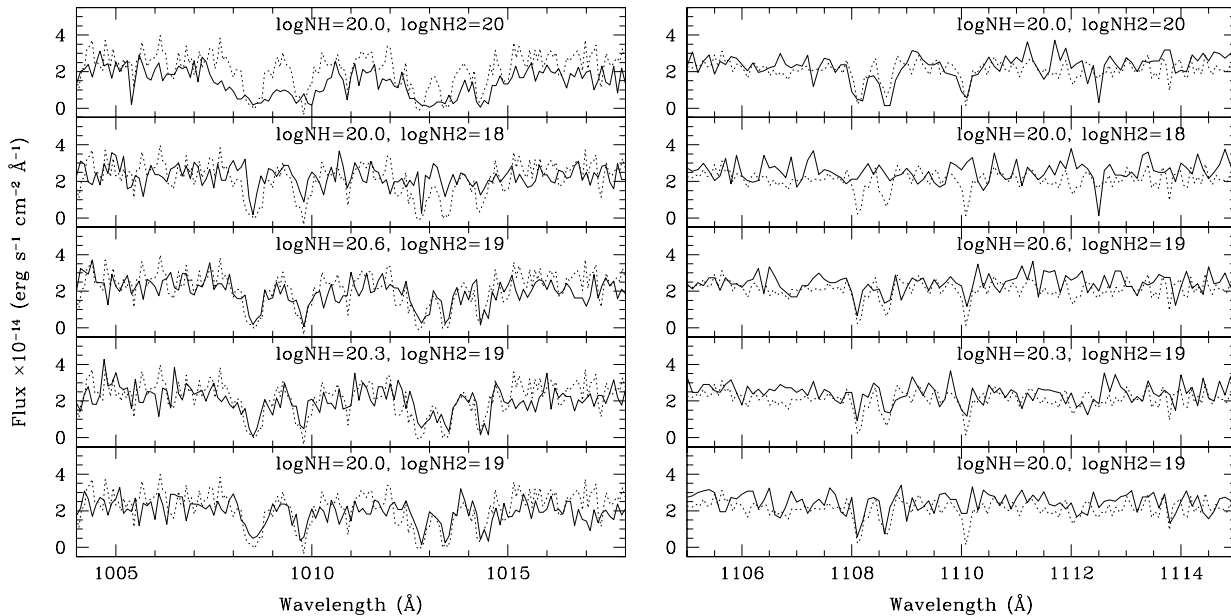


Fig. 2.— Two portions of all photon FUSE spectrum (LiF 1A and 1B channels) of PNG 135.9+55.9 that include prominent interstellar lines of H_2 are plotted with a dotted line. Overplotted are modelled spectra that assume a flat underlying spectrum of intensity $3 \times 10^{-14} \text{ erg s}^{-1} \text{ cm}^{-2} \text{ Å}^{-1}$ and different column densities of neutral and molecular hydrogen.

line protrudes more than can be accounted for by the models, even if column densities exceeding $\log N_H = 20.3$ are considered. If this is the case, then the upper limit to the flux from the $\text{He II } \lambda 1025.273$ is $\leq 4.4 \times 10^{-16} \text{ erg cm}^{-2} \text{ s}^{-1}$, according to the model fit that is described in Sect. 4.2.

In the optical range, we discovered signatures of the central object in the form of absorption lines at the wavelengths of hydrogen and helium lines. These features were not previously noted because our new spectra have higher S/N (by a factor of 3) and higher spectral resolution than all of our previous spectra. As an experiment, we degraded our new CFHT spectra to the resolution that we used before, and the absorption features almost disappeared, leaving marginal traces only in higher members of the Balmer series. Our previous observations also used a wider slit, substantially increasing the nebular contribution and possibly widening the emission lines.

As detailed in the Table 1, we obtained seven optical spectra of PNG 135.9+55.9 during one night. The observations were primarily designed

to obtain deep spectrophotometric data in far optical UV for study of Ne ions located there and other possible faint emission lines from the nebula in the integrated spectrum. These will be discussed in a subsequent publication concerning the nebular characteristics. Here we concentrate on the features due to the central star. Even a simple eye inspection of the co-added spectrum immediately attracted our attention to the dips around higher Balmer series lines, which are clearly not centered on the emission lines. An analysis of the individual spectra revealed that the center of the absorption component varies, indicating large radial velocity shifts.

In principle, our observing technique and equipment are not ideal for detecting radial velocity variations. The use of a grism spectrograph, with a nonlinear dispersion, the large range of telescope inclination angles spanned by the observations, and the variable slit angle combined to scatter the absolute zero point of the wavelength scale among the spectra by up to 10 Å . However, all of our measurements of absorption components in the central star spectrum that are relevant to this study where

made relative to corresponding nebular emission line components, which effectively eliminates possible problems.

4. Quantitative analysis of the stellar core of PN G 135.9+55.9

4.1. First determinations of the radial velocity variations

Initial estimates of the radial velocities (RVs) were obtained by de-blending the line profiles with the fit routines of the *gnuplot* program. A Gaussian profile was assumed for the emission component (from the nebula). A Voigt profile was taken for the absorption component, as it is better suited to fit a broad white dwarf-like absorption component. We succeeded in separating the components for the lines where we had enough signal, enough continuum around the lines, and an absorption component sufficiently strong to be resolved. This concerns primarily $H\gamma$, $H\delta$, and $H\epsilon$, where de-blending worked fine for all seven spectra (i.e. for different orbital phases), returning consistent parameters of the measured lines from one line to another and from spectrum to spectrum. To reduce the number of free parameters, we performed a simultaneous fit of all spectra. The FWHM of the Gaussian used to fit the emission lines and the parameters of the Lorentzian fit to the photospheric absorption were held fixed, because these values should remain constant, while all other parameters were allowed to vary from spectrum to spectrum.

The imperfections of wavelength calibration were eliminated by measuring the radial velocities of the absorption components relative to their emission counterparts, which we suppose to be constant in general, and on such short time scale in particular, as is also evident from our previous observations (Richer et al. 2002). The corresponding measurements of the absorption components along with epochs of observation are presented in the second and sixth columns of Table 1. Clearly, the radial velocity variations of the absorption components of these three lines are consistent with each other, and vary strongly on a timescale of a few hours. Before analyzing their time dependence, i.e. periodic nature, let us consider atmospheric models of the central star and estimate radial velocities from the absorption line fits.

4.2. Model atmosphere calculations

The model atmosphere spectra used for our analysis were computed with the NLTE code PRO2 developed by Werner (1986). The basic assumptions are those of static, plane-parallel atmospheres in hydrostatic and radiative equilibrium. As described in Werner (1986) and Werner & Dreizler (1999), the accelerated lambda iteration (ALI) method is used to solve the set of non-linear equations.

The basic parameters, effective temperature and surface gravity, were determined with the grid of model atmospheres composed of hydrogen and helium calculated by Napiwotzki (1999) for the analysis of planetary nebulae central stars. Extensive model atoms for hydrogen and helium (He I and He II) were used (cf. Napiwotzki 1999, for details). Line profiles of the hydrogen Balmer and Lyman lines and the He II lines were computed using extended VCS broadening tables (Vidal, Cooper & Smith 1973) provided by Lemke (1997) and Schöning & Butler (1989), respectively.

4.3. The gravity of the central star from model atmosphere analysis

It has now become a standard technique to determine both the temperature and gravity of central stars of planetary nebulae or of hot white dwarfs from a simultaneous fit of the Balmer series (e.g. Napiwotzki 1999) or Lyman series (Barstow et al. 2001).

In our FUSE spectrum, only the $Ly\beta$ line has a reasonable signal-to-noise. Higher members of the Lyman series fall in the SiC channels, which are characterized by lower effective area and hence lower S/N. However, the analysis of the $Ly\beta$ line is problematic as well, because major parts of the line profile are contaminated by geocoronal emission or absorption caused by interstellar hydrogen molecules.

The best opportunity for parameter estimation is offered by the hydrogen Balmer lines in the optical spectrum, although these lines are also contaminated by the strong emission coming from the nebula. The emission subsides toward higher members of the Balmer series, while the decline of the photospheric absorption lines is less pronounced. Thus, it was possible to fit five Balmer lines (from $H\gamma$ to H_9).

Table 1: RV measurements from the optical spectra. The heliocentric Julian date of the center of the exposures and the RV shifts relative to the nebular emission lines are given^b.

spectrum number	HJD-2,450,000	RV atm. model fit / 5 lines composite	RV de-blending		
			H γ	H δ	H ϵ
457	2760.80249	-204 ± 25	-95	-136	-180
466	2760.90086	269 ± 28	257	236	365
467	2760.92412	179 ± 25	208	220	258
471	2760.95986	-53 ± 60	23	-7	0
472	2760.98410	-59 ± 60	28	16	-36
476	2761.01893	111 ± 28	178	138	164
477	2761.04169	246 ± 28	229	236	264

^bRV errors estimated from measurements of emission line component does not exceed ± 10 km/sec.

The model atmosphere analysis was done with the programme FITSB2, which was originally developed to analyze the spectra of double-lined white dwarfs from the SPY project Napiwotzki et al. (2003, 2004). However, this programme is also well-suited for the analysis of the spectra of single-lined binaries. FITSB2 performs a simultaneous fit of spectra covering different orbital phases, i.e., all available information is combined into the parameter determination procedure. Fit results are stellar parameters and RVs (a more detailed discussion is given in Napiwotzki et al. 2004). Two He II lines (4540 Å and 4686 Å) are visible as well and enabled us to estimate the helium abundance.

We used the nebular emission lines to correct the wavelength calibration as described in Sect. 4.1. Since the emission components of the higher Balmer lines are weak, individual wavelength measurements become less accurate. Thus we performed an average over all spectra and calculated wavelength corrections from a simple linear fit and applied this for all lines higher than H γ . Deviations of individual measurements for H γ , H δ , and H ϵ , which are most important for the RV determination, never exceeded 10 km/s.

Due to the nebular contamination of the available spectra, it was not possible to determine both the temperature and gravity from the available spectra. Thus, we kept the temperature fixed during the fitting procedure and determined only the surface gravity. We considered T_{eff} values in the range 80000 K to 150000 K. The results are listed in Table 2. Due to potential problems with degradation of the line profile by orbital smearing (cf.

discussion below), we restricted the model atmosphere fit to the three spectra with the largest RV shifts (shown in Fig. 3). These were probably taken close to quadrature phases, for which the rate of change of RV and thus the orbital smearing is smallest.

Below 90000 K and above 120000 K the quality of the Balmer line fits degrades significantly. The analysis of the nebular spectrum of PN G 135.9+55.9 indicates a central star temperature of at least 100,000 K (Tovmassian et al. 2001, Richer et al. 2002). Taking into account the detection of the [Ne V] 3426 Å line (Jacoby et al. 2002, Stasińska et al in preparation) an even higher temperature is required, unless an additional source of EUV photons is present in this system. These combined constraints are best fulfilled by the solution with $T_{\text{eff}} = 120000$ K and $\log g = 5.35$. The atmosphere model fits to the portions of spectra with largest RV shifts are presented in Fig 3. The formal fit uncertainty in $\log g$ for a given value of T_{eff} is 0.07 dex. As discussed in Napiwotzki (1999), the formal errors computed by the fit procedures are usually too optimistic. Thus we made an estimate of the external error as described in Napiwotzki (1999) and derived an error limit of 0.22 dex. The position of PN G 135.9+55.9 in the $\log g, T_{\text{eff}}$ plane is shown in Fig. 4. Although the helium lines are weak and almost completely filled in by the nebular emission lines, we could derive an estimate of the helium abundance (Fig. 3). The fit yielded $\log n_{\text{He}}/n_{\text{H}} = -1.0$, i.e., close to the value derived for the nebula. The error of the abundance measurement can be estimated from the scatter

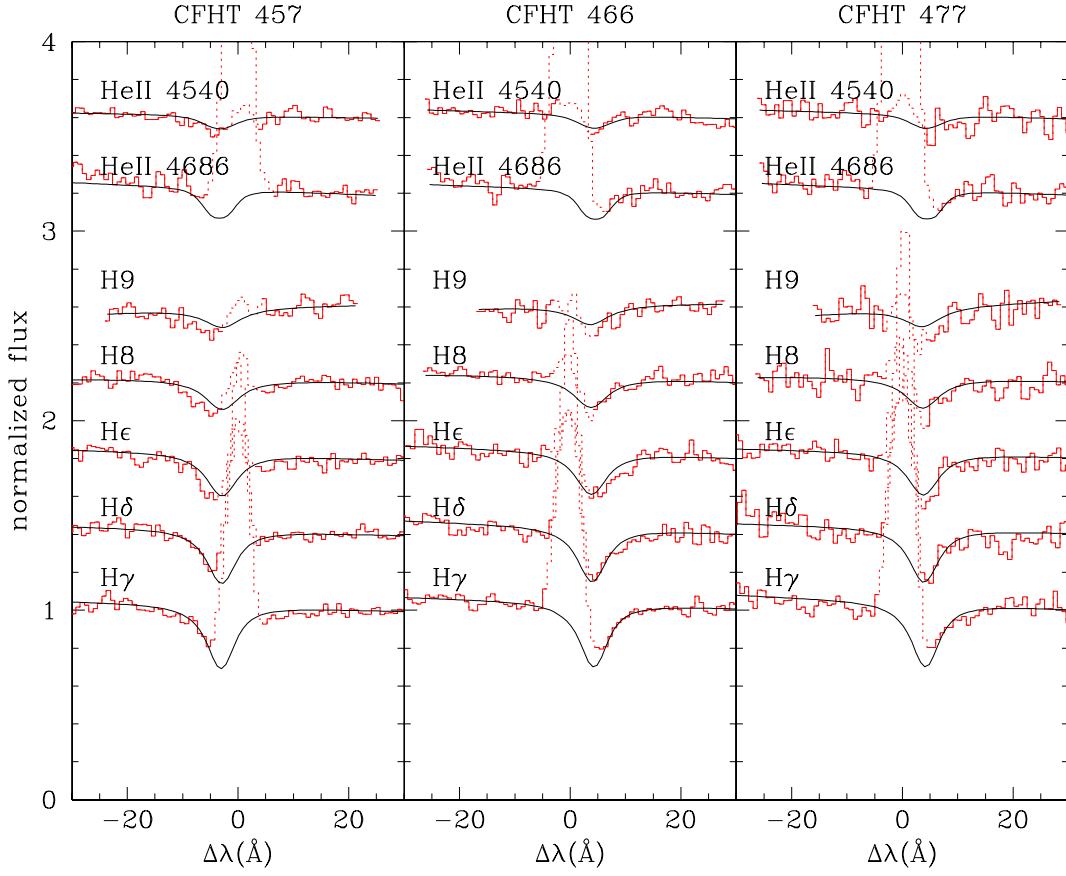


Fig. 3.— A model atmosphere fit (solid line) to the optical spectra (histogram) taken during the phases with largest RV shifts. The dotted lines indicate parts of the spectra which were excluded from the fit.

between the individual spectra, which amounts to 0.2 dex.

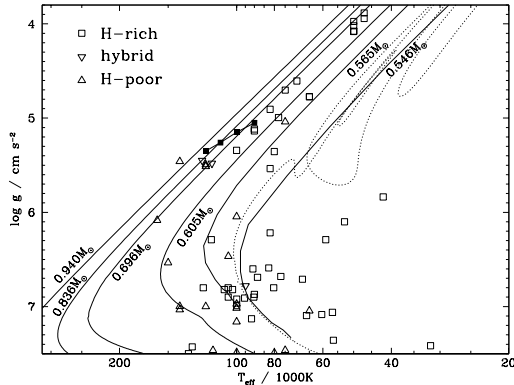


Fig. 4.— Post-AGB evolutionary tracks for different stellar masses from the grid of Blöcker (1995) and Schönberner (1983) in the $(\log g, T_{\text{eff}})$ plane. The $0.524M_{\odot}$ post-AGB track discussed in the text is drawn as dotted line. The connected filled symbols indicate the positions of the central star of PN G 135.9+55.9 according to the solutions ranging from 90000 K to 120000 K. Open symbols are central stars of planetary nebulae and other post-AGB objects taken from the literature (Napiwotzki 1999)

The $\text{Ly}\beta$ line from the FUSE spectra is sensitive to gravity as well. However, the total exposure time of the FUSE spectrum amounts to 8.5 hours, distributed over 11.7 hours. This is much longer than any plausible orbital period (Sect 4.4) and it is reasonable to assume that we have approximately equal coverage of all orbital phases. This means that orbital smearing is the dominant broadening mechanism for the observed $\text{Ly}\beta$ line, even more important than the pressure broadening of the photospheric absorption line. We adopted the atmospheric parameters derived above ($T_{\text{eff}} = 120,000\text{K}$ and $\log g = 5.35$) for the fit shown in Fig. 5.

The photospheric $\text{Ly}\beta$ line is contaminated by interstellar absorption that we must take it into account. In addition to the discussion in Section 3.1 the column density of the atomic interstellar hydrogen can be determined from the red wing of the $\text{Ly}\beta$ line which is most sensitive to the interstellar absorption (cf. Fig. 5, note the gap between the terrestrial airglow lines of H I and O I).

Best agreement is achieved with a column density $N_{\text{H}} = 3 \times 10^{20}\text{cm}^{-2}$. Acceptable fits are derived for the range $2 \times 10^{20}\text{cm}^{-2} \leq N_{\text{H}} \leq 5 \times 10^{20}\text{cm}^{-2}$. This coincides perfectly with estimates of N_{H} from other wavelength regions (Section 3.1).

As mentioned above the line widths depend upon the assumed amplitude of the orbital motion, K_1 . We obtained the best fit for a velocity amplitude of 450 km/s. Acceptable fits could be produced for velocity amplitudes in the range from 250 km/s to 600 km/s. Thus the result from the fit of the $\text{Ly}\beta$ line is in agreement with the orbital solutions discussed in the next section.

4.4. Investigating the periodicity of the radial variations

As mentioned above, FITSB2 is not only able to derive the stellar parameters, but can measure RVs as well. We measured RVs for all CFHT spectra with temperature and gravity now fixed at the value $T_{\text{eff}} = 120000\text{K}$ and $\log g = 5.35$ derived above. The Balmer lines $H\gamma$ to H9 and the two He II lines were used for the RV determination. The results are summarized in Table 1. Formal errors provided by the fit procedure are relatively small ($\approx 15\text{km/s}$). We added to these uncertainties an additional 10 km/s to account for the remaining uncertainty in the wavelength scale. The RV measurements for the conjunction spectra 471 and 472 are problematic, because the RV fits basically rely on the invisibility of the photospheric Balmer lines. We estimated an RV error of 60 km/s from the scatter of the results derived using different methods.

The RV variation has a clearly periodic nature. However, the sparseness of data does not allow an unambiguous determination of the orbital period. Fig. 6 shows a “power spectrum” which was produced by fitting RV sine-like curves for a range of periods. The resulting fit quality, measured by χ^2 , is plotted in Fig. 6. Since the number of data points is low and the measurements are difficult due to the strong nebular emission lines, we held the system velocity fixed at the value $\text{RV} = -193\text{km/s}$ derived by Richer et al. (2003). The best fit quality is obtained for a period of $0^{\text{d}}150$ ($3^{\text{h}}6$). The corresponding RV curve is shown in the bottom panel of Fig. 7. For this solution, the two RV measurements close to conjunction (phase 0.75) are problematic, because they lie in a “for-

Table 2: Results of the model atmosphere fits of the quadrature spectra 457, 466, and 477 for several values of T_{eff} . Masses and radii were derived from an interpolation in the post-AGB tracks in Fig. 4.

T_{eff} K	$\log g$ cm s^{-2}	$\log(n_{\text{He}}/n_{\text{H}})$	M/M_{\odot}	R/R_{\odot}
80000	4.99		0.62	0.42
90000	5.05		0.68	0.41
100000	5.15		0.75	0.38
110000	5.26		0.83	0.35
120000	5.35	-1.00	0.88	0.33
130000	5.39		0.96	0.33
150000	5.56		1.02	0.28

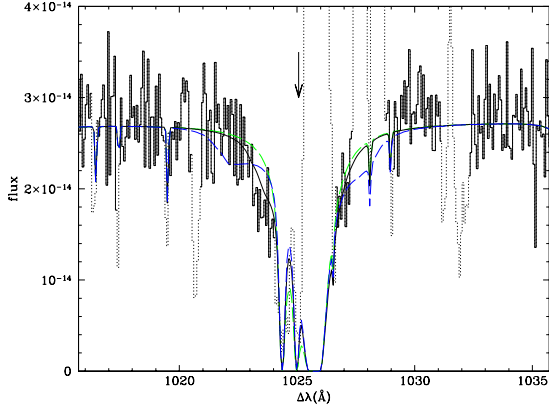


Fig. 5.— Model atmosphere fit to the Ly β line of PNG 135.9+55.9. The histogram is the observed all photon spectrum. Only those parts shown with a continuous line were used to fit both the stellar profile and determine the interstellar absorption. The bold, solid line shows the best fit to the stellar absorption including all of the interstellar contributions and smearing effects (where K_1 is the radial velocity of the ionizing star = 450 km/s). The long dashed lines are the spectra resulting for $K_1 = 0$ km/s (green) and 900 km/s (blue). The arrow indicates the center of the photospheric Ly β line.

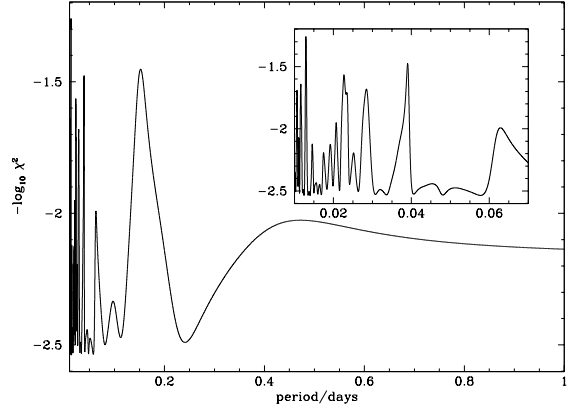


Fig. 6.— The power spectrum for the FITSB2 RV measurements from Table 1. The inset gives a more detailed view for shorter periods. Periods below 0.01 d (≈ 15 min) can be ruled out, because these periods would be much smaller than our exposure time.

bidden” area of this diagram. These points are less problematic for the solutions with shorter periods of 0^d039 (0^h94) and 0^d063 (1^h5), presented in the top and middle panels of Fig. 7, respectively. Orbital parameters are detailed in Table 3. The amplitudes from the best fit solutions for 0^d039 d and 0^d063 are quite high. We calculated alternative (“minimal”) solutions by assuming that the orbital amplitudes correspond to the maximum observed RV shifts (after correction for orbital smearing; see below). A solution with a period significantly longer than 4 h can be ruled out. Apart from the formal χ^2 values shown in Fig. 6, simply consider the large RV shift between spectra 457 and 466: 470 km/s in just 2^h3!

For the two shortest period solutions found (0^d063 and 0^d039), note that the exposure times of 30 min extend over a large range of phases. Thus, smearing due to the orbital RV variations must be taken into account as a major problem. This could cast doubt upon whether any absorption line features should be observable at all. We made simple simulations of this effect and found that, although the line profiles are indeed seriously distorted, line profiles similar to those observed can still be produced, but that the measured RV values are severe underestimates of the real RVs. The difference between the real and measured RVs are smallest for

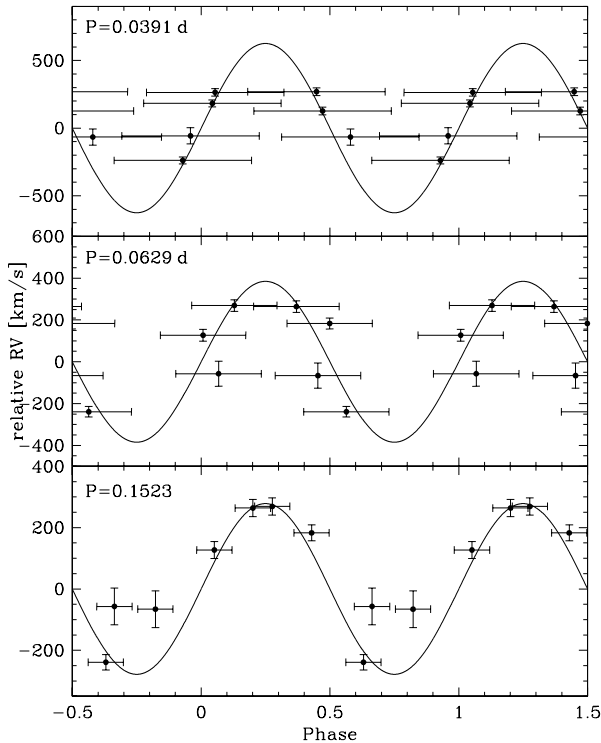


Fig. 7.— Radial velocity curves for three possible orbital periods. The error bars in the phase coordinate correspond to the duration of the individual exposures.

the exposures centered on the quadrature phases of largest RV shift. We calculated approximate corrections for these phases by measuring the displacement of the line cores in our simulated spectra. Results are 124 km/s for the 0^d.039 orbit and 59 km/s for 0^d.062. The correction for 0^d.151 is negligible within uncertainties (10 km/s). We can conclude that the orbital period cannot be longer than 4 h, but a time series of spectra with much shorter exposure times are needed for an unambiguous period determination.

It has long been speculated that many planetary nebulae have binary nuclei. There are models that invoke binarity of the central object in order to explain the morphology of certain types of planetary nebulae (Soker 2002). Evolutionary models of close binaries require that a fraction of the systems going through the common envelope phase

form a planetary nebula (Yungelson et al. 1993; Iben & Tutukov 1989). However, the number of observationally-confirmed binary cores in planetary nebulae is relatively small. Nonetheless, there are reasons to believe that many more of them are indeed binaries (De Marco et al. 2003), though many probably have relatively long periods. The discovery that the central star of PN G 135.9+55.9 is a close binary is thus very important in this context.

5. The extinction of PN G 135.9+55.9

With our FUSE data, we are able to further address the question of the reddening of PN G 135.9+55.9. In our previous studies, the reddening was derived from a comparison of the observed hydrogen and helium emission line ratios with those given by recombination theory. Richer et al. (2002) noted that the reddening of PN G 135.9+55.9 was modest. The $H\gamma/H\beta$ and $H\delta/H\beta$ line ratios gave an $E(B-V)$ of 0.3–0.35 mag (the $H\alpha/H\beta$ ratio was apparently variable and indicated even lower reddening). The He II λ 5412/4686 ratio implied a negative reddening.

From the FUSE data, we can estimate the extinction suffered by the object by fitting the flux distribution of PN G 135.9+55.9 from the far UV to the near IR. This is shown in Fig. 8. In this figure, the observed energy distribution of PN G 135.9+55.9 from the far UV to the near IR is represented by open squares. The fluxes were measured in narrow bands free of any significant lines ($\approx 3-4 \text{ \AA}$ in the far UV and $\approx 20 \text{ \AA}$ in the optical). The dashed lines are continuum fits to the spectrophotometric data. The solid line is the model of the central star described above for a temperature of 120 000 K and $\log g = 5.35$. The slope of the observed UV spectrum (1000–1200 \AA) is consistent with the model, but shifted downwards due to the interstellar extinction. If we correct for interstellar reddening using the tables from (Fitzpatrick 1999) and assume the standard value $R_V = 3.1$ and $E(B-V) = 0.03$ mag (Jacoby et al. 2002), we effectively recover ≈ 0.45 mag of flux, but this is not enough to compensate all losses in the UV. Increasing $E(B-V)$ to 0.045 mag yields a better fit overall, but, at that point, the optical fluxes show some excess in comparison to the model, while the UV flux is still somewhat short

Table 3: Orbital solutions for a $0.55M_{\odot}$ primary and the three possible periods. The set of parameters on the left corresponds to the fit results displayed in Fig. 7. For the set of parameters on the right, we assumed that the orbital velocity corresponds to the maximum of the measured RV shifts, corrected for the effect of orbital smearing. The subscripts 1 and 2 correspond to parameters for the ionizing and companion stars, respectively.

Best fit solution						“Minimal” solution				
P (d)	v_{orb} (km/s)	$M_2 \sin i$ (M_{\odot})	a (R_{\odot})	R_1^{Roche} (R_{\odot})	R_2^{Roche} (R_{\odot})	v_{orb} (km/s)	$M_2 \sin i$ (M_{\odot})	a (R_{\odot})	R_1^{Roche} (R_{\odot})	R_2^{Roche} (R_{\odot})
0.039	590	1.55	0.63	0.19	0.30	390	0.73	0.54	0.19	0.22
0.063	380	0.92	0.77	0.26	0.33	320	0.69	0.73	0.26	0.29
0.151	265	0.82	1.35	0.47	0.56					

of it. If we also take into account the nebular continuum at a temperature of 30 000 K from our best fit photoionization models of the nebula (Richer et al. 2002, Sect. 8), which contributes primarily in the optical range (dash-dot line in Fig. 8), then the fit is improved (filled black squares). Much better results are obtained using $R_V = 2.3$ and $E(B - V) = 0.045$ mag (open circles). This could mean that the dust towards PNG 135.9+55.9 is non-canonical. This may indeed be the case since the line of sight toward PNG 135.9+55.9 is not necessarily characterized by the canonical value $R_V = 3.1$ (e.g., Barbaro et al. 2001). Moreover, the far UV part of Fitzpatrick’s reddening curve is actually an extrapolation of near UV data into the FUSE range.

Another way to estimate the reddening is to use the H I column density derived from our FUSE spectrum and convert it into a reddening using the relation between $E(B - V)$ and $N_{\text{H I}}$ of Burstein & Heiles (1978). For $N_{\text{H I}} = 3 \times 10^{20}$, we find $E(B - V) = 0.01$ mag.

These values are somewhat smaller than the reddening derived by Richer et al. (2002) from the Balmer decrement. Those reddenings were derived in the usual way, comparing the observed emission line ratios with the theoretical ones and assuming emission under case B at a nebular temperature of 30 000 K. However, no account was taken of the underlying stellar absorption. When this effect is properly taken into account (Stasińska et al. in preparation), the reddening derived from the Balmer decrement is compatible with the values obtained from our FUSE spectrum.

Thus we confirm that the reddening, and hence

extinction, of PNG 135.9+55.9 is indeed low. In the following, we adopt a value of $E(B - V) = 0.04$ mag, but none of our conclusions would be significantly affected should the real value be slightly different.

6. The distance and age of PNG 135.9+55.9

Having an estimate of the stellar gravity and a measurement of the apparent magnitude of the central star, we can estimate the distance d to the object using the expression:

$$d = 1.11(M_{\star}F_V 10^{0.4m_V}/g)^{0.5}$$

where d is in kiloparsecs, M_{\star} is the stellar mass in solar units, F_V is the model stellar flux in the V band in $10^8 \text{ erg cm}^{-2} \text{ s}^{-1} \text{ \AA}^{-1}$, and m_V is the observed stellar magnitude corrected for nebular contribution and for extinction. This method to evaluate the distances to PNe has been discussed extensively by Napiwotzki (2001) and there are strong arguments that such spectroscopic distances are reliable (within the uncertainties). To evaluate the distance to our object, we take the observed magnitude $m_V = 17.9$ mag from Richer et al. (2002), assume a reddening of $E(B - V) = 0.04$ mag, and apply a correction of 0.15 mag for the nebular continuum contribution, as derived from photoionization models described in Richer et al. (2002). The stellar flux for the model with $T_{\text{eff}} = 120000$ K and $\log g = 5.35$ is $7.07 \cdot 10^8 \text{ erg cm}^{-2} \text{ s}^{-1} \text{ \AA}^{-1}$. Adopting a stellar mass of $0.55M_{\odot}$, we find a distance to PNG 135.9+55.9 of 17.8 kpc. Had we adopted a stellar mass of $0.88M_{\odot}$, as indicated by Fig. 4 and listed in Table 2, we would have found a distance of 22.6 kpc.

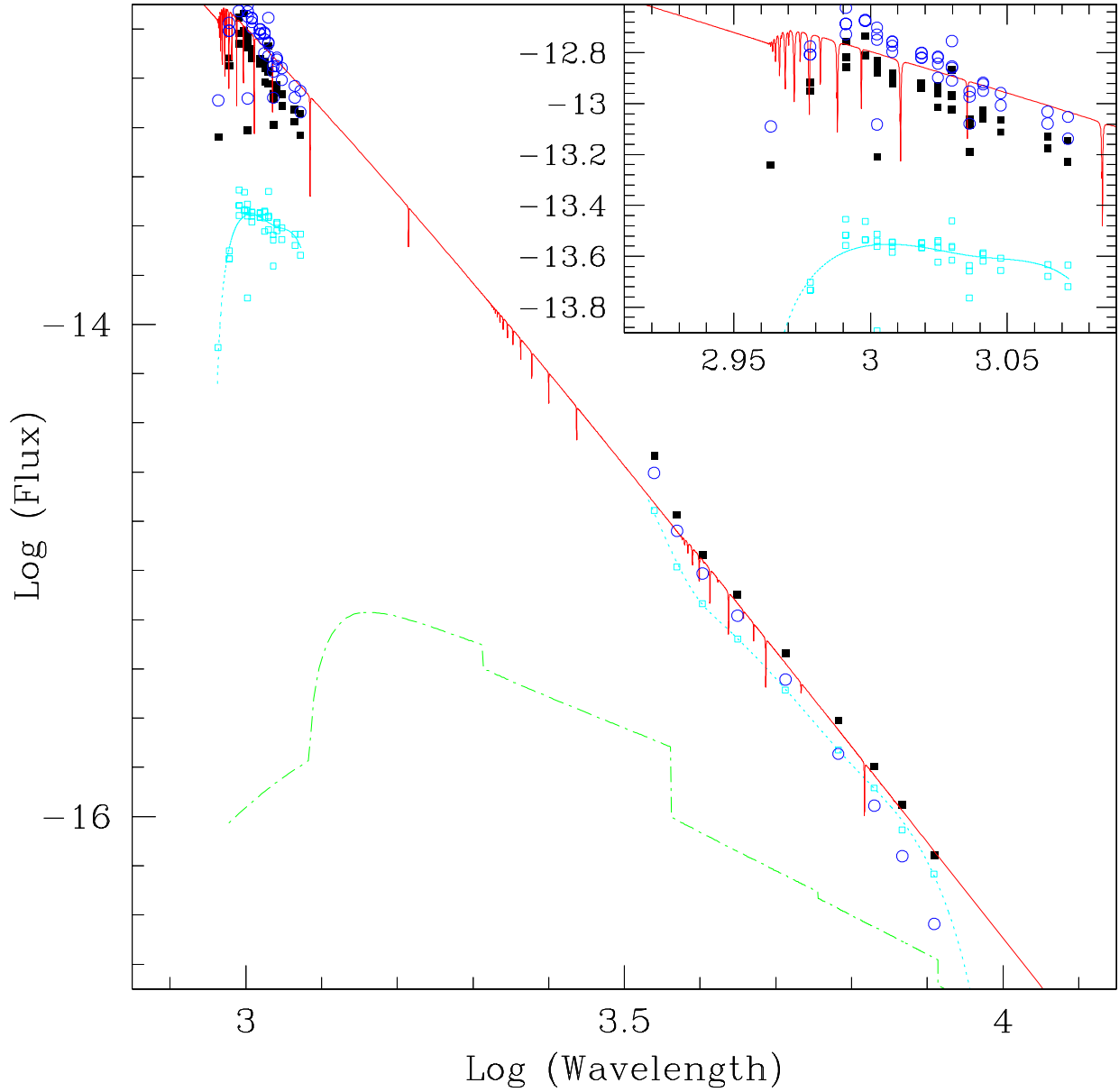


Fig. 8.— The flux distribution of PNG 135.9+55.9 from far UV to near IR. The open squares are the observed fluxes. The dashed lines are continuum fits to the observed data. Fluxes corrected for interstellar extinction are represented by filled squares ($R_V = 3.1$, $E(B - V) = 0.045$ mag). The dot-dash line is the expected contribution from the nebula (see text). The open circles are the extinction-corrected data ($R_V = 2.3$) after subtraction of the nebular component. The central star model with 120 000 K and $\log g = 5.35$ is presented as a solid line. The model is normalized to the raw flux observed at 4000 Å.

Assuming that the stellar temperature is only 90000 K and taking the values of $\log g$ and M_* from Table 2, we find $d = 24.2$ kpc, while assuming a stellar temperature of 150000 K, we find $d = 20.6$ kpc. The largest contribution to the error budget is the uncertainty in $\log g$ for a fixed T_{eff} , which amounts to an uncertainty of 5 kpc in the distance.

In any case, our present estimates of the distance are consistent with PNG 135.9+55.9 being located in the Galactic halo. Note that the values of the distance obtained in this way are roughly consistent with the ones obtained previously (Tovmassian et al. 2001; Richer et al. 2002), which were based upon nebular properties (flux and dimensions), whereas the present determination relies *only* on the fit of the stellar spectrum. This indicates that we are progressively getting a coherent picture of the nebula.

On the other hand, the discovery of the compact binary nature of the nucleus of PNG 135.9+55.9 introduces new challenges in interpretation of the evolutionary path of this unique object. For further discussion, a rough estimate of the age of the planetary nebula is useful. The expansion time, t_{exp} , of the planetary nebula is generally computed as $t_{\text{exp}} = R_{\text{out}}/v_{\text{exp}}$, where R_{out} is the outer radius of the nebula and v_{exp} is its expansion velocity. This is of course a simplistic approach, since it is known that the expansion velocity should vary during the course of the nebular evolution (see e.g. the dynamical models of Villaver, Manchado & García-Segura 2002) and that the epoch of the ejection of the nebula does not necessarily coincide with the evolution of the central star off the AGB. In the case of PNG 135.9+55.9 the expansion time measures the time since a final mass loss episode triggered by common envelope interaction of the binary stellar core (Sect. 7). The transition phase from the AGB to a hot post-AGB was certainly strongly affected by the binary evolution. Nevertheless, an estimate of the nebula expansion time provides a valuable constraint, which is especially important in the context of close binary stellar evolution. We adopt the nebular size determined by Richer et al. (2002) and an expansion velocity of 30 km s⁻¹ as found by Richer et al. (2003). For a distance of 17.8 kpc, we find a nebular expansion time of 15800 yr. Using this rough age estimate, the position of the object in the

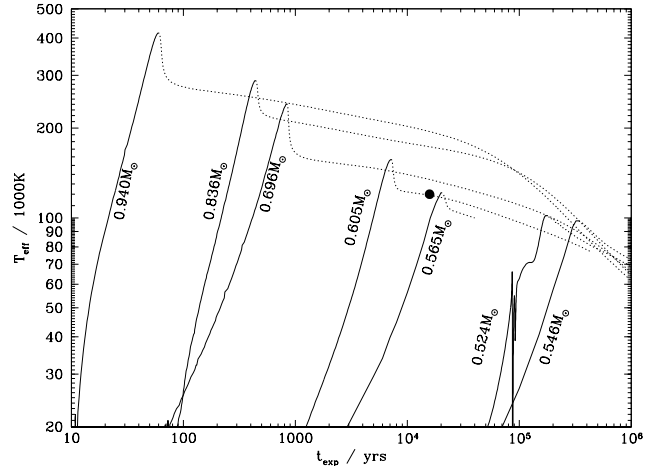


Fig. 9.— Post-AGB evolutionary tracks for different stellar masses interpolated from grid of Blöcker (1995); Schönberner (1983) in the (T_{eff} , t_{exp}) plane. Tracks are plotted with solid/dotted lines for the parts before/after maximum temperature. The position of PNG 135.9+55.9 is marked for the estimated values of $T_{\text{eff}} = 120\,000$ K and $t_{\text{exp}} = 16\,000$ yr.

(T_{eff} , t_{exp}) diagram (Figure 9) can be compared with that of model stellar tracks of various masses (Blöcker 1995; Schönberner 1983). The position of PNG 135.9+55.9 in Fig. 4 indicates that the comparison must be made with the part of the tracks that lie prior to the temperature maximum (solid lines in Fig. 9). We find that the position of PNG 135.9+55.9 is consistent with a mass of the ionizing star around $0.57 M_{\odot}$.

7. Discussion: The status of the stellar core of PNG 135.9+55.9

7.1. The ionizing star

As described above, we derived the surface gravity of PNG 135.9+55.9 from fits of the Balmer lines of selected optical spectra. Because of nebular contamination of the optical spectra, we cannot determine both the temperature and gravity, so we adopted $T_{\text{eff}} = 120\,000$ K based upon the analysis of the nebula (Stasińska et al. in preparation). The resulting gravity is $\log g = 5.35$. From a comparison with evolutionary tracks of H-burning central stars of planetary nebulae (Fig. 4) we esti-

mated a mass of $0.88M_{\odot}$. This value is at variance with the expected properties of a Population II central star. Three lines of evidence point towards a Population II nature of PN G 135.9+55.9: the large height above the Galactic plane ($z = 14.8$ kpc for $d = 17.8$ kpc), the high radial velocity ($RV = -193$ km/s), and the very low metal abundances derived from the analysis of the planetary nebula and the far-UV spectrum of the central star (Stasińska et al., in preparation).

Known post-AGB stars of Population II have low masses ($\approx 0.55M_{\odot}$; e.g., Moehler et al. 1998), which is explained by the small mass of their progenitors. One could argue that problems caused by the orbital motion and the contamination by the nebula emission lines cause a systematic shift of the fit results. However, from a comparison of observed and synthetic spectra, we conclude that a gravity much higher than that given by our fits can be ruled out, because the resulting lines would be much broader than observed. Our estimate of the effective temperature is based upon the analysis of the nebular spectrum. If an additional source of hard ionizing photons were present in this system, (e.g. resulting from interaction between the components of the binary system), the nebular spectrum would actually overestimate the temperature of the ionizing star. Lower temperatures would result in lower mass estimates (Table 2) in better agreement with the expected mass of a Population II central star.

Due to the obvious Population II nature of PN G 135.9+55.9, in the subsequent discussion we shall adopt a mass of $0.55M_{\odot}$ for the ionizing star. A low mass is also supported by the relatively large kinematic age of the nebula. If the mass of the ionizing star were really as high as the estimates derived from Fig. 4, e.g., $0.9M_{\odot}$, the time interval between the tip of the AGB and the hottest point of the post-AGB evolution would be of order of only 100 years, much shorter than the estimated nebular expansion age of 16000 years. The observed nebular age is in much better agreement with a mass of $\approx 0.57M_{\odot}$ (or lower), for which transition times are ≈ 20000 yrs (or longer). Note that the common envelope phase very likely abbreviated the post-AGB evolution.

How might we explain the apparent discrepancy between the observed and expected parameters of the ionizing star? The progenitor almost certainly

went through a common envelope phase, which drove it out of thermal equilibrium. In this case, the relations used to derive the stellar mass from $\log g$ and T_{eff} do not apply. However, relaxation happens on the thermal time scale of the post-AGB envelope, which is given by

$$t_{\text{th}} = G \frac{M M_{\text{env}}}{R L},$$

where G is the gravitational constant, M the mass of the central star, M_{env} the mass of the stellar envelope, R the stellar radius, and L the stellar luminosity. For the derived stellar parameters and an adopted mass for the post-AGB envelope of $M_{\text{env}} = 10^{-2}M_{\odot}$, the resulting thermal time scale amounts to only ≈ 30 years. Since the real envelope mass is probably smaller (cf. Fig. 3 of Schönberner 1983), this can be considered an upper limit. The short relaxation time makes it unlikely that we observe the star precisely in this stage.

A more plausible explanation is that the post-AGB star experienced a late thermal pulse (shell helium flash) after emerging from the common envelope phase. Stars suffering a late thermal pulse evolve back to cooler temperatures and then replicate the previous post-AGB evolution (Iben et al. 1983; Schönberner 1983; Bloeker 1995). The evolutionary speed and luminosity during this second phase can be quite different from the ones in the first phase. As an illustration, we plotted in Fig. 4 the track computed by Bloeker (1995) for a $0.52M_{\odot}$ post-AGB star, which experiences two late thermal pulses. The resulting track spans a wide range of gravities and luminosities, whose details depend upon the precise mass and thermal pulse phase. Most importantly, the time scales for this kind of evolution are thousands to tens of thousands of years, making it much more likely to catch a star in one of these phases.

7.2. The companion star

The short orbital period and large semiamplitude of the RV that we detect imply that the other component of the binary system should be a rather massive star. The mass function can be used to derive lower limits to the mass of the unseen companion, if the mass of the visible star is known (Table 3). In the case of the 3:6 solution we derive a minimum companion mass of $0.82M_{\odot}$ for a

$0.55M_{\odot}$ ionizing star ($1.01M_{\odot}$ for a $0.88M_{\odot}$ ionizing star). The best fit orbits for the shorter period solutions indicate even higher companion masses. However, the “minimal” solutions yield lower limits of $\approx 0.70M_{\odot}$. Thus the companion must be a relatively massive star.

Note that the system is physically small. The separation between both stars amounts to only $1.35R_{\odot}$ for the $3^{\text{h}}6$ solution and the $0.55M_{\odot}$ ionizing star (Table 3). The Roche lobe of the companion has a size of $0.56R_{\odot}$. A metal-poor $0.6M_{\odot}$ main sequence star has a radius of $0.55R_{\odot}$ (Baraffe et al. 1997), almost filling its Roche lobe if the period is 3.6 h and overfilling it for the other solutions. However, the orbital solutions require more massive companions that have even larger radii and would therefore not fit into their Roche lobes, so a main sequence companion appears unlikely. Further evidence against a main sequence companion comes from the binary system BEUMa. It consists of a hot post-AGB star with parameters similar to that of PN G 135.9+55.9 (Liebert et al. 1995) and a K dwarf companion. However, this system has a much wider orbit ($P = 2^{\text{d}}29$) than PN G 135.9+55.9, yet it still shows a spectacular reflection effect producing a forest of RV variable emission lines from the heated surface of the companion (Ferguson & James 1994). The absence of these lines in our spectra is another strong argument in favor of a compact companion, i.e., a white dwarf or a neutron star. A photometric monitoring campaign to search for variability should be able to provide final evidence against (or for) a main sequence companion. Note that the ionizing star fills a significant fraction of its Roche lobe as well (Tables 2 and 3). The $T_{\text{eff}} = 120000\text{ K}$, $\log g = 5.35$ solution corresponds to a radius of $0.26R_{\odot}$ compared to a Roche lobe of $0.47R_{\odot}$ in the 3.6 h orbit. According to the temperature-radius relation from the $0.546M_{\odot}$ track of Schönberner (1983) the ionizing star completely filled its Roche lobe when it had a temperature of 50000 K. This represents the minimum temperature of the ionizing star for the stellar core of PN G 135.9+55.9 to become a detached system. Model predictions indicate that the central star fills or overfills its Roche lobe for the 1.6 h and 0.94 h solutions, respectively.

In the standard picture of the common envelope phase the companion spirals in until enough

orbital energy is released to eject the envelope (Webbink 1984). For a system with a companion as massive as in the case of PN G 135.9+55.9, one would expect that only a moderate spiral in would be necessary, producing a relatively wide system. We used standard assumptions for the common envelope phase (formula A.14 of Nelemans et al. 2001, with $\alpha_{\text{CE}}\lambda = 2$) to estimate the initial separation of the PN G 135.9+55.9 system before the final common envelope. For the $3^{\text{h}}6$ orbit we calculated an initial separation of only $3.6R_{\odot}$ (initial/final mass: $0.85M_{\odot}/0.55M_{\odot}$, companion mass: $0.8M_{\odot}$). This is an impossible value, because this would indicate that interaction started shortly after the main sequence phase, preventing the star from becoming the central star of a planetary nebula. Thus it is difficult to explain the formation of the PN G 135.9+55.9 system with standard assumptions. On the other hand this means that PN G 135.9+55.9 could provide an important test of our understanding of common envelope evolution.

If the companion is a compact star, the binary will merge in less than 1 Gyr due to the loss of energy and angular momentum caused by gravitational wave radiation. Our estimates from the mass function show that the companion should be rather massive and it is quite possible that the sum of the masses of this system exceeds the Chandrasekhar limit for white dwarfs ($1.4M_{\odot}$). Such systems are proposed as progenitors of SN Ia (Webbink 1984; Iben & Tutukov 1989). The SPY project (Supernovae Ia Progenitor survey) Napiwotzki et al. (2001, 2003) performed a radial velocity survey of white dwarfs for potential SN Ia progenitors. To date, only one possible candidate system was detected (Napiwotzki et al. 2003), illustrating how rare these systems are. If it can be shown that the core of PN G 135.9+55.9 is massive enough to qualify as SN Ia progenitor, this would provide the bonus that additional information about the formation of such systems is available from the chemistry and morphology of the planetary nebula.

8. Conclusions

We have presented new optical and far-UV spectra of the central star of the very metal-poor planetary nebula PN G 135.9+55.9. The photo-

spheric Balmer lines visible in the optical spectra enabled us to determine the surface gravity from a model atmosphere analysis. For a temperature of $T_{\text{eff}} = 120000\text{ K}$ (as indicated by the nebular emission lines), we derived a gravity of $\log g = 5.35$ and a photospheric helium abundance $\log n_{\text{He}}/n_{\text{H}} = -1.0$. Our model atmosphere spectrum also fits the UV Ly β line profile observed in the FUSE spectrum satisfactorily given that the Ly β line is contaminated by interstellar lines and suffers from severe smearing effects due to the orbital RV variations.

Comparing the above values of T_{eff} and $\log g$ with those from evolutionary tracks in the $\log g$ - T_{eff} plane yields a mass of $0.88M_{\odot}$ for the ionizing star, if one adopts standard H-burning post-AGB stellar tracks. This result is in contrast with the Population II nature of this object, indicated by its metallicity (Tovmassian et al. 2001, Richer et al 2002, Jacoby et al. 2002, Stasińska et al., in preparation), location in the galactic halo, and its large radial velocity (Richer et al. 2003). We argue that the real mass of the ionizing star of PNG 135.9+55.9 is close to the typical masses of Population II post-AGB stars: $\approx 0.55M_{\odot}$. Since the stellar core of PNG 135.9+55.9 is a close binary the formation of the planetary nebula is likely to have happened during a phase of common envelope evolution.

A comparison of a model spectrum calculated for appropriate stellar parameters and the observed FUSE and optical fluxes indicates a reddening of $E_{B-V} = 0.04\text{ mag}$. This relatively small value is in agreement with the expectations for an object at high galactic latitudes ($b = +56^{\circ}$). This low reddening is also in agreement with the estimates the interstellar atomic and molecular hydrogen column densities towards PNG 135.9+55.9 based upon the FUSE observations. Allowing for extinction, we obtain a distance for PNG 135.9+55.9 from a comparison of its measured flux in the V band and model atmosphere fluxes. The result is $\approx 18\text{ kpc}$, which places PNG 135.9+55.9 15 kpc above the galactic plane. The kinematical age of the nebula is ≈ 16000 years, in rough agreement with expectations if the central star mass is of order $0.55M_{\odot}$. This expansion age argues against a more massive central star, e.g., $0.9M_{\odot}$, since the expected post-AGB age of such a star is only 100 years.

The optical spectra reveal large radial velocity variations of the stellar absorption lines, obviously caused by orbital movement in a close binary system. Since the observations were not designed for the measurement of a binary orbit, the phase coverage and the wavelength calibration are not optimal. However, we show that the orbital period must be less than 4 hours (our three best solutions are 0^h94, 1^h5, and 3^h6 hours) and the minimum (half-)amplitude of the radial velocity amounts to 250 km/s. The companion remains invisible in the spectra during all orbital phases. Our preliminary orbital solutions indicate a companion mass of $\approx 0.9M_{\odot}$. A solid lower limit is $0.6M_{\odot}$. It is very unlikely that the companion is a main sequence star, because we would then expect a strong reflection effect producing very strong emission lines from the irradiated hemisphere of the main sequence star. That these are not observed in the optical spectra indicates that the companion is most probably a white dwarf or a neutron star.

Due to the short orbital period (four hours or less) the system will merge in less than one Gyr, if the companion is a compact star. If a companion mass exceeding $0.85M_{\odot}$ can be confirmed, the total mass of the stellar binary core would exceed the Chandrasekhar limit and this system would qualify as a potential progenitor of a type Ia supernova. New observations, with shorter exposure times and longer time coverage, will be needed in order to establish a definitive orbital period and other parameters for the binary system.

G.T. acknowledges CNRS/CONACyT grant and hospitality of Observatoire de Meudon during his visit. GS and MR acknowledge CONACYT grant 37214-E. R.N. acknowledges support by an PPARC Advanced Fellowship. We thank Martine Mouchet for help with the interstellar molecular hydrogen lines and Slawomir Górny for extending the grid of interpolated post-AGB evolutionary tracks. R.N. thanks Philipp Podsiadlowski and Martin Beers for useful comments on this system. Special thanks to Klaus Schenker for many helpful suggestions and discussions. This paper is based upon observations made with the NASA-CNES-CSA Far Ultraviolet Spectroscopic Explorer. FUSE is operated for NASA by the Johns Hopkins University under NASA contract

NAS5-32985.

REFERENCES

- Bannister, N. P., Barstow, M. A., Holberg, J. B., Bruhweiler, F. C., 2003, MNRAS, 341, 477
- Baraffe, I., Chabrier, G., Allard, F. & Hauschildt, P.H. 1997, A&A 327 1054
- Barbaro, G., Mazzei, P., Morbidelli, L., Patriarchi, P., Perinotto, M., 2001, A&A 365, 157
- Barstow, M.A., Holberg, J.B., Hubeny, I., et al. 2001, MNRAS 330, 425
- Blöcker, T., 1995, A&A, 299, 755
- Burstein, D., Heiles, C., 1978, ApJ 255, 40
- De Marco, O., Bond, H. E., Harmer, D., Fleming, A. J., 2004, ApJ 602, L93
- Dickey, J.M. & Lockman, F.J., 1990, ARA&A 28, 215
- Feldman, P.D., Sahnou, D.J., Kruk, J.W., Murphy, E.M., Moos, H. W., 2001, JGR, 106, 8119
- Ferguson, D. H. & James, T. A. 1994, ApJS 94, 723
- Fitzpatrick, E. L., 1999, PASP, 111, 63
- Froning, C. S., Long, K. S., Drew, J. E., Knigge, C., Proga, D., 2001, ApJ, 562, 963
- Górny, S. K., Stasińska, G., Tyłenda, R., 1997, A&A, 318, 256
- Iben, I.Jr., Kaler, J. B., Truran, J. W., Renzini, A. 1983, ApJ 264 605
- Iben, I., & Tutukov, A. V., ApJS 54, 335 in Planetary Nebulae, Proceedings of the 131st symposium of the IAU. Ed S. Torres-Peimbert, p 505
- Jacoby, G. H., Feldmeier, J., Claver, C. F., Garnavich, P. M., Noriega-Crespo, A., et al. 2002, AJ, 124, 33490
- Le Fèvre, O., Crampton, D., Felenbok, P., & Monnet, G. 1994, A&A, 282, 325
- Lemke, M., 1997, A&AS, 122, 285
- Liebert, J., Tweedy, R. W., Napiwotzki, R. & Fulbright, M. S. 1995, ApJ 441, 424
- McCandliss, S.R., 2003, PASP, 115, 651
- Moehler, S., Landsman, W., & Napiwotzki, R. 1998, A&A 335, 510
- Moos, H.W., 2000, BAAS, 197, 6801
- Napiwotzki, R. 1999, A&A 350, 101
- Napiwotzki, R. 2001, A&A 367, 973
- Napiwotzki, R., Christlieb, N., Drechsel, C., et al. 2001, AN 322, 411
- Napiwotzki, R., Christlieb, N., Drechsel, C., et al. 2003, ESO Messenger 112, 25
- Napiwotzki, R., Yungelson, L., Nelemans, G. et al. 2004, in: 'Spectroscopically and spatially resolving the components of close binary stars', eds. R.W. Hilditch, H. Hensberge & K. Pavlovski (ASP Conf. Series), in press (astro-ph/0403595)
- Nelemans, G., Yungelson, L. R., Portegies Zwart, F., & Verbunt, F. 2001, A&A 365, 491
- Oke, J. B. 1990, AJ, 99, 1621
- Richer, M. G., Tovmassian, G.H., Stasińska, et al. 2002, A&A, 395, 929
- Richer, M. G., López, J.A., Steffen, W. Tovmassian, G., Stasińska, G., Echevarría, J., 2003, A&A, 410, 901
- Sahnou, D., Hart, H., Dixon, V., Oegerle, B., Murphy, E., Kriss, J., and FUSE team, 2002, <http://fuse.pha.jhu.edu/analysis/IDH/IDH.html>
- Schönberner, D., 1983, ApJ, 272, 708
- Schöning, T. & Butler, K., 1989, A&AS, 78, 51
- Soker, N., 2002, MNRAS, 330, 481
- Tovmassian, G. H., Stasińska, G., Chavushyan, V. H., Zharikov, S. V., Gutierrez, C., Prada, F. 2001, A&A, 370, 456
- Vidal C.R., Cooper J., Smith E.W., 1973, ApJS 25, 37
- Villaver, E., Manchado, A., & García-Segura, G., 2002, ApJ 581, 1204

- Webbink, R. F. 1984, ApJ 277, 355
- Werner, K. 1986, A&A 161, 177
- Werner, K., & Dreizler, S. 1999, Journal of Computational and Applied Math. 109, 65
- Wolff, B., Kruk, J. W., Koester, D., et al. 2001, A&A, 373, 674
- Yungelson, L. R., Tutukov, A. V., Livio, M., 1993, ApJ, 418, 794